Electronic Supplementary Information for

Highly conductive and robust anion conductor via synergistic manipulation in intra- and inter-laminate of layered double hydroxide nanosheets

Xueyi He,[ab] Li Cao,[ab] Guangwei He,[ab] Anqi Zhao,[ab] Xunli Mao,[ab] Tong Huang,[ab] Yan Li,[ab] Hong Wu,[ab] Jie Sun[a] and Zhongyi Jiang*[ab]

[a] *Key Laboratory for Green Chemical Technology of Ministry of Education, School of Chemical Engineering and Technology, Tianjin University, Tianjin 300072, China.*

[b] *Collaborative Innovation Center of Chemical Science and Engineering (Tianjin), Tianjin, 300072, China.*

Corresponding author: Zhongyi Jiang, E−mail: zhyjiang@tju.edu.cn

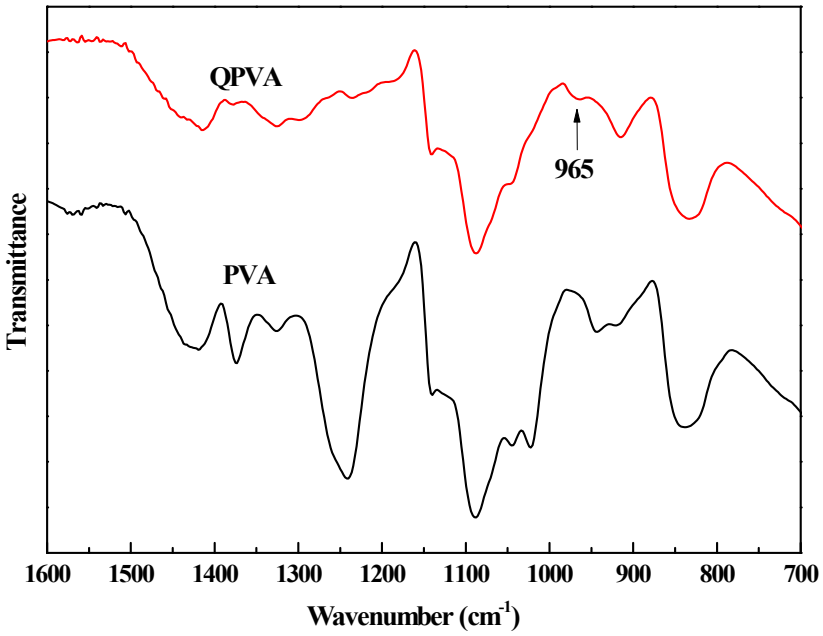

Fig. S1 FTIR spectra of QPVA and PVA

The chemical composition of QPVA was confirmed by the FTIR spectrum (Fig. S1). A new adsorption band at 965 cm^{-1} appeared in the FTIR spectrum of QPVA, corresponding to the stretching vibration of aliphatic C-N bond[1]. The mass fraction of nitrogen (n = 1.07%) in QPVA was obtained by elemental analysis. The degree of substitution (DS) could thus be calculated according to the following equation:

$$DS(\%) = \frac{n/14}{n/14 + (100 - 195.5n/14)/44} \times 100 \qquad (1)$$

The DS of QPVA was calculated to be 3.8%.

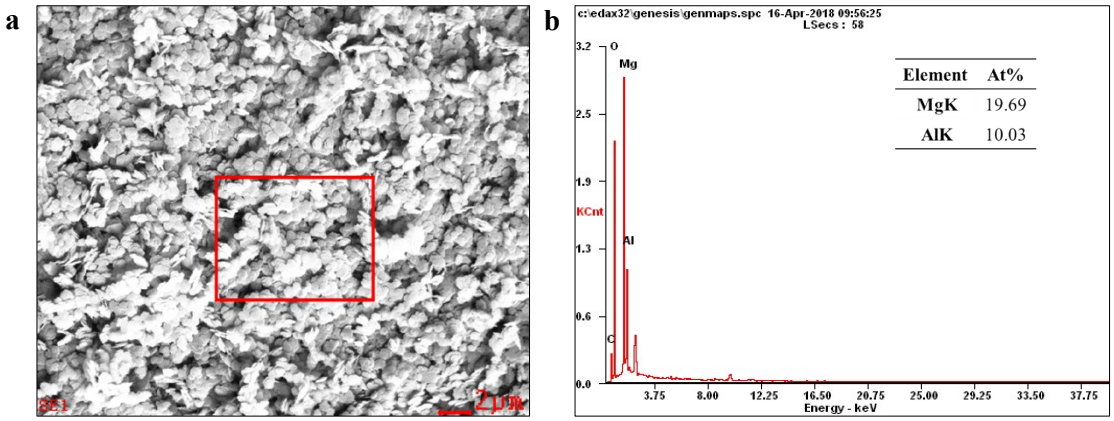

Fig. S2 (a) SEM image and (b) EDX for MgAl-CO_3-LDH. The Mg/Al ratio was calculated to be 2.0.

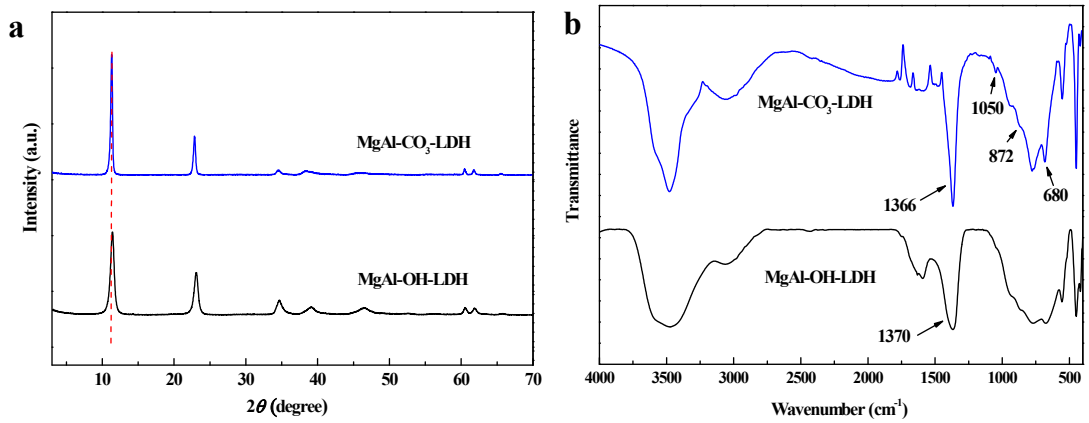

Fig. S3. (a) XRD patterns and (b) FTIR spectra of MgAl-CO_3-LDH and MgAl-OH-LDH.

The MgAl-OH-LDH platelets was prepared using MgAl-CO_3-LDH as the starting material. As illustrated in Fig. S3, the XRD patterns indicated a slight decrease in the interlayer distance (from 0.773 nm to 0.768 nm) of MgAl-OH-LDH compared with MgAl-CO_3-LDH platelets. In accordance with the previous report[2], a strong band in the FTIR spectrum of MgAl-OH-LDH could be observed at 1370 cm^{-1} similar to MgAl-CO_3-LDH. Meanwhile, a slight contamination of CO_2 resulted in weak vibration bands (1050 cm^{-1} and 680 cm^{-1}) of CO_3^{2-} species.

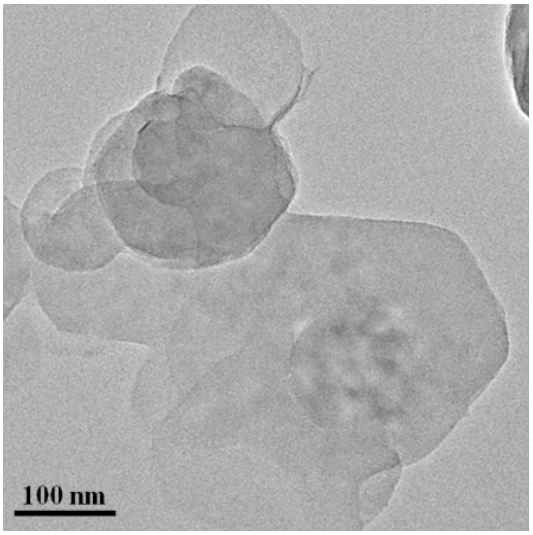

Fig. S4 TEM image of LDH nanosheets

The colloidal suspension of LDH was dropped onto a copper mesh and vacuum-dried for TEM observation. The exfoliated LDH nanosheets restacked after the evaporation of formamide, which was clearly shown in Fig. S4.

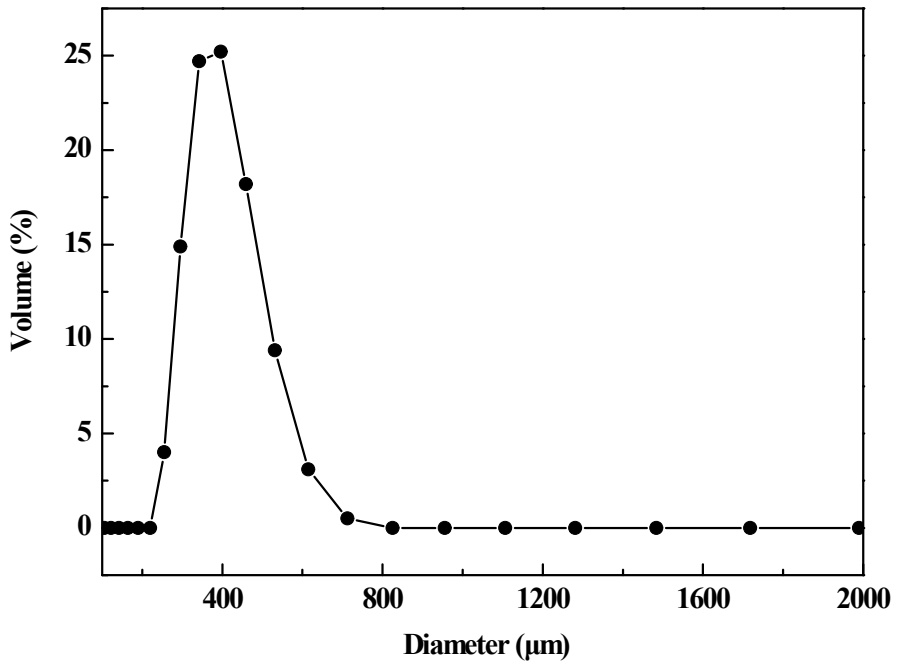

Fig. S5 Equivalent size distribution of exfoliated MgAl-LDH nanosheets in formamide

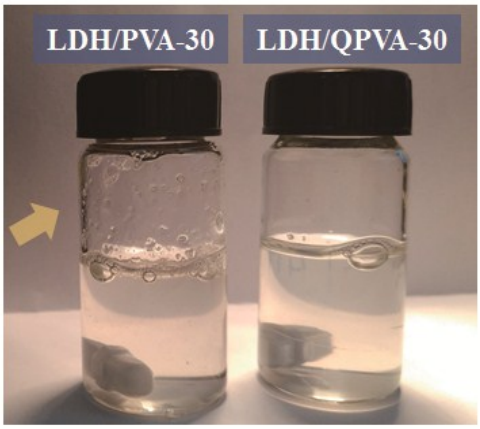

Fig. S6 Digital picture of LDH colloidal suspensions with PVA and QPVA.

Table S1 Zeta potential of the LDH/QPVA colloidal suspensions with different QPVA content

QPVA content (%)	0	10	20	30	40	100
Zeta potential (mV)	64.1	60.1	53.1	44.2	40.1	12.9

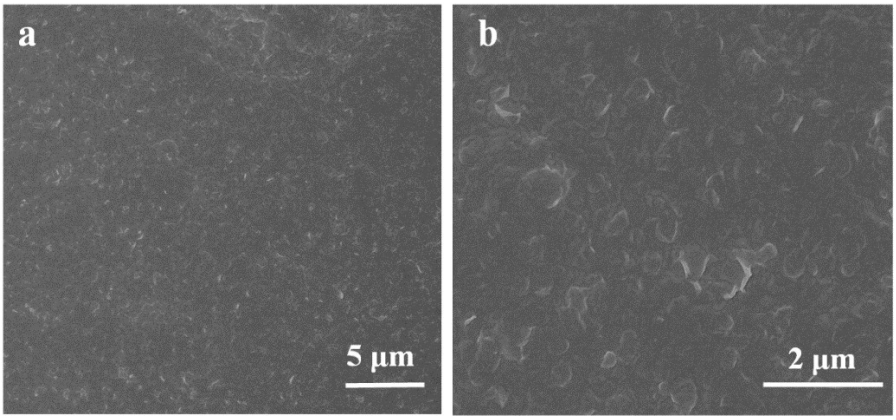

Fig. S7 SEM plane views of the LDH/QPVA-20 membrane at (a) low and (b) high magnifications

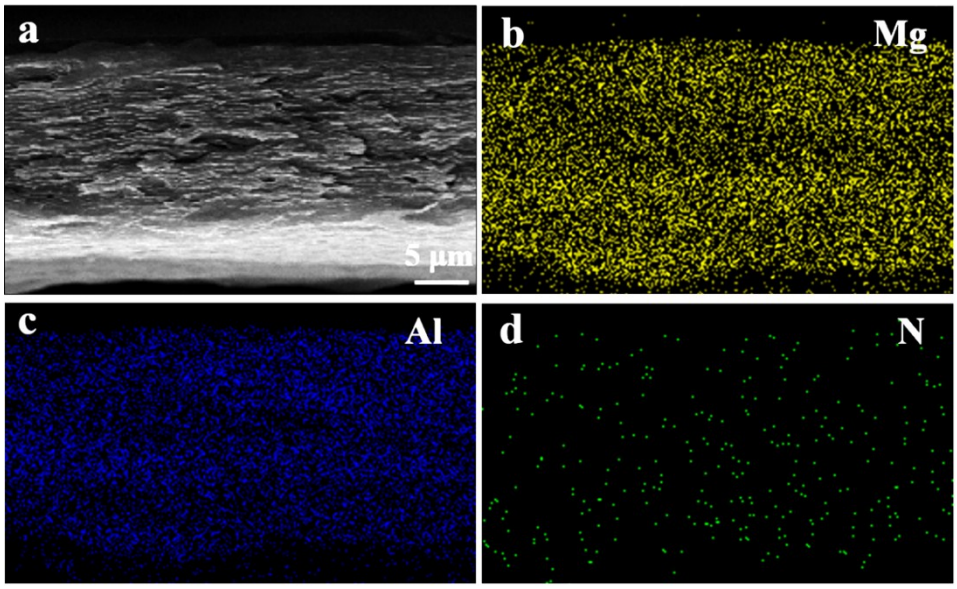

Fig. S8 (a) SEM image of the LDH(Cl^-)/QPVA-30 membrane and EDX mapping of (b) Mg, (c) Al and (d) N elements in the membrane.

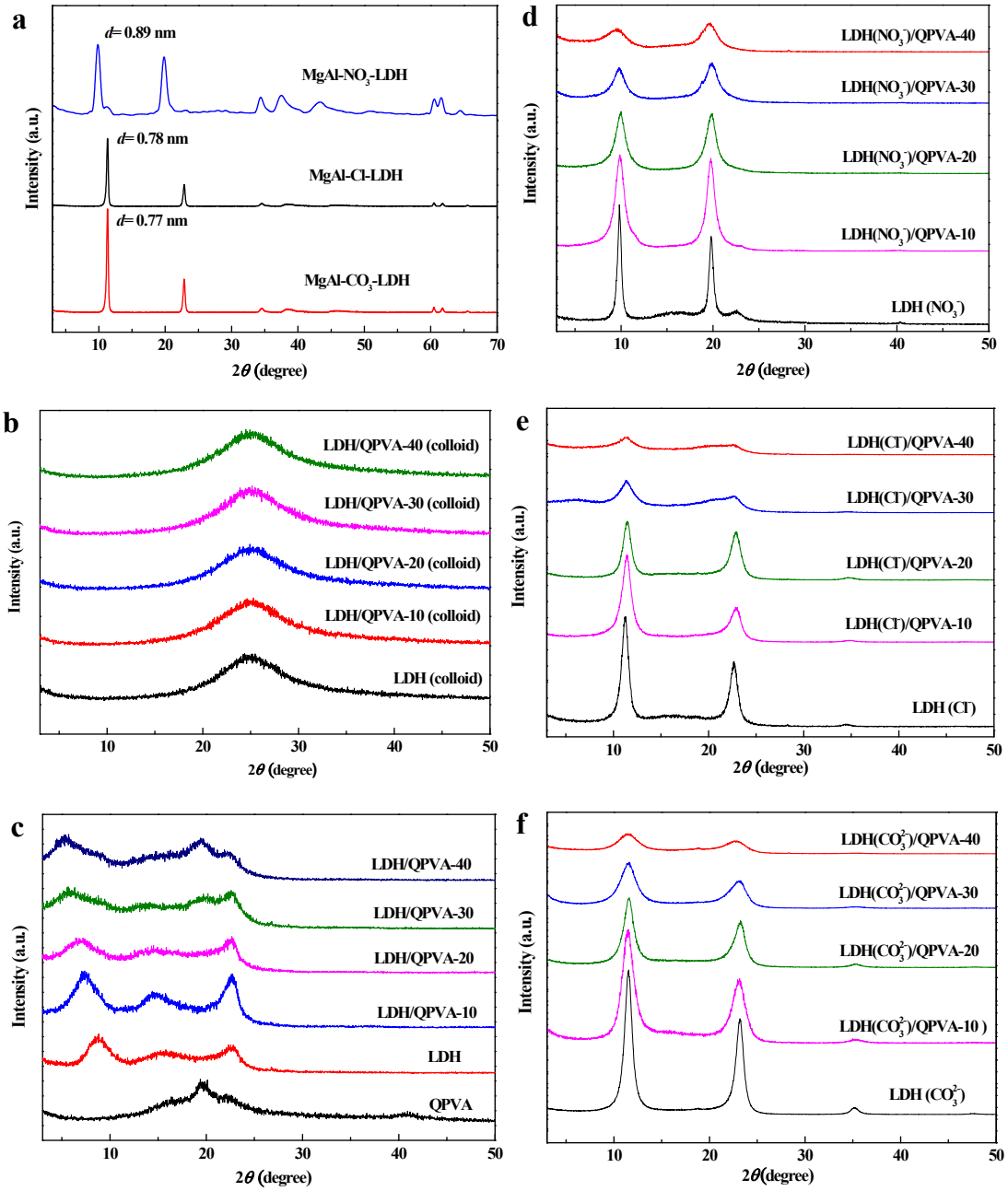

Fig. S9 XRD patterns of the (a) LDH platelets, (b) LDH, LDH/QPVA colloidal aggregates, (c) LDH, QPVA, LDH/QPVA membranes as well as (d) NO_3^-, (e) Cl^- and (f) CO_3^{2-} intercalated membranes.

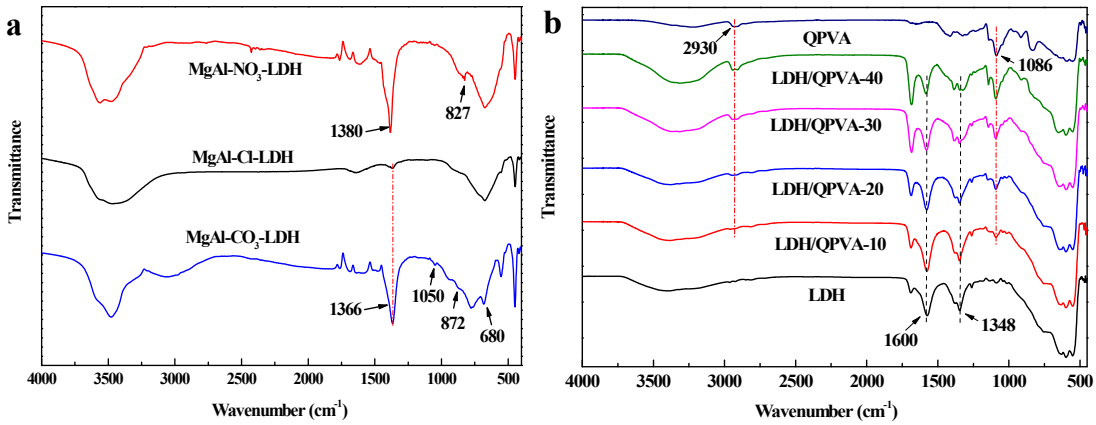

Fig. S10 FTIR spectra of the (a) LDH platelets, (b) QPVA, LDH and LDH/QPVA membranes

The FTIR spectra (Fig. S10) identified the intercalated anions inside the LDHs. The FTIR spectrum of MgAl-CO_3-LDH showed characteristic peaks at 1366, 1050, 872 and 680 cm^{-1}, assigning to the vibration of CO_3^{2-}. In terms of the MgAl-NO_3-LDH, characteristic peaks at 1380 and 827 cm^{-1} corresponded to the vibration of NO_3^-. Due to a small amount of CO_3^{2-} be incorporated during the salt-acid treatment, characteristic peak (1366 cm^{-1}) relating to the vibration of CO_3^{2-} could be observed in the spectrum of MgAl-Cl-LDH[3]. In Fig. S10b, the LDH/QPVA membranes with increasing QPVA content showed more intensive peaks at 2930 and 1086 cm^{-1} assigning to the stretching vibration of C-H and C-O inside the polymer while less intensive peaks at 1348 cm^{-1} relating to the stretching vibration of NO_3^-. Moreover, pronounced adsorption at 1600 cm^{-1} corresponding to the bending vibration of water could be observed in the LDH-based membranes[2].

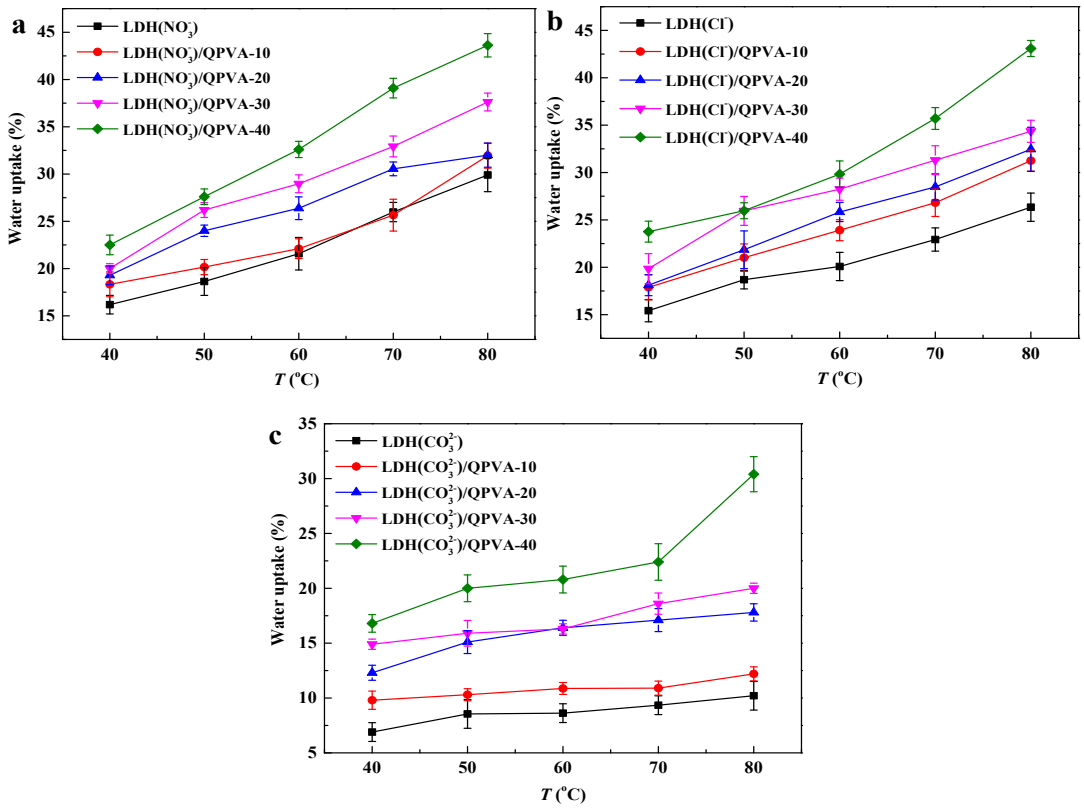

Fig. S11 Water uptake of the pure LDH membrane and composite membranes at different temperatures with (a) NO_3^-, (b) Cl^- and (c) CO_3^{2-} intercalation

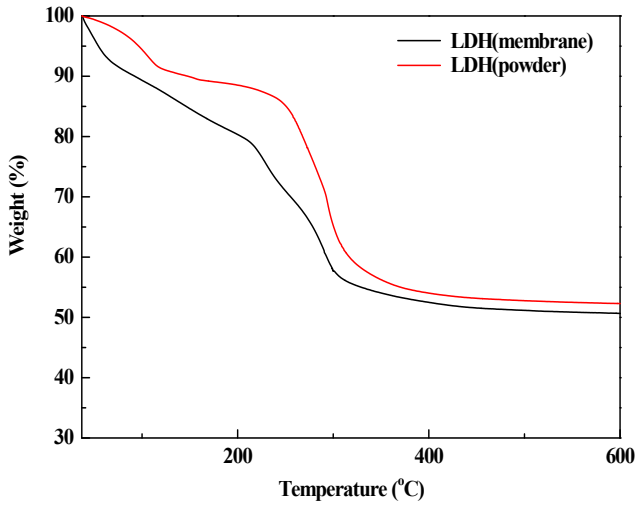

Fig. S12 TGA curves of the LDH platelets and the LDH membrane

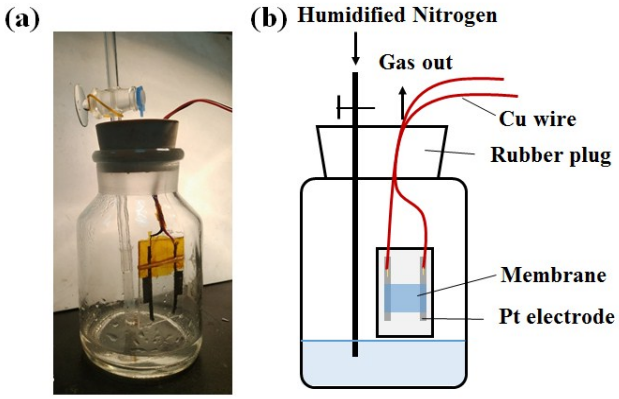

Fig. S13. (a) Digital picture and (b) schematic illustration of the experimental device.

The conductive performance of LDH-based membranes with OH^- intercalation was measured based on the device illustrated in Fig. S13. Before testing, plenty of distilled water was added to the bottle. Nitrogen (99.999% purity) was humidified and bubbled through the liquid to remove the air inside the bottle. Exposed to a continuous gas flow, the membrane was fixed on the Pt electrodes and heated by water vapor to a certain temperature. After putting the device in an oven, the membrane sample (LDH-based membrane with CO_3^{2-} intercalation) was equilibrated at 40 ^oC for 5 h and then a direct current of 0.1 mA was applied to the membrane by the electrochemical workstation (PARSTAT 3000A AMETEK Inc.). After a period of time, the sample was probed by the two Pt electrodes and in-plane conductivity was tested. 12 h later, there was negligible variation in anion conductivity of the membrane sample (Fig. S14), indicating the conversion of interlayer CO_3^{2-} to OH^-.

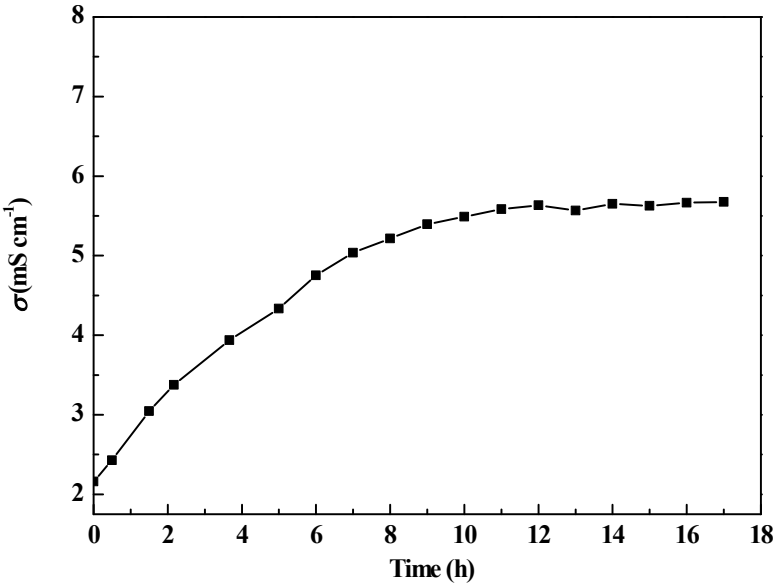

Fig. S14. Changes in ion conductivity of LDH(CO_3^{2-})/QPVA-10 during applying the direct current at 40 °C, 100% RH.

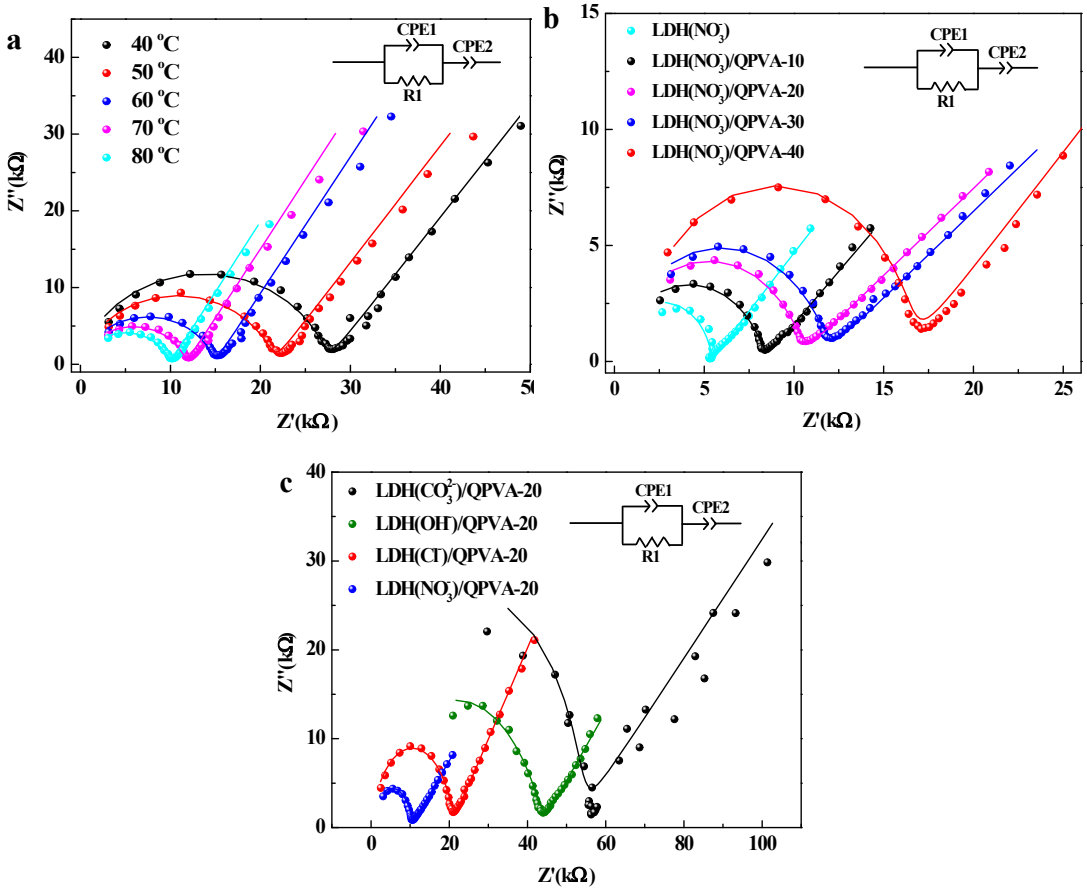

Fig. S15 Nyquist plots of (a) the LDH(NO_3^-)/QPVA-20 membrane under 98% RH at different

temperatures, (b) the LDH(NO_3^-) and LDH(NO_3^-)/QPVA membranes at 80 °C, 98% RH, (c) the LDH/QPVA-20 membrane with NO_3^-, Cl^- and CO_3^{2-} intercalation at 80 °C, 98% RH and the LDH(OH^-)/QPVA-20 membrane at 80 °C, 100% RH. The equivalent circuit is presented inside the figures. The solid spheres represent experimental results and the solid lines the fitting results of the data. Equivalent circuit parameters are listed in Table S2.

Table S2 Equivalent circuit parameters determined by fitting of the responses

Element	$R1(\Omega)$	CPE1		$C(F)^a$	$T(^oC)$
		$Y_o(S\ s^\alpha)$	α		
LDH(NO_3^-)/QPVA-20	28,070	9.94×10^{-10}	0.88	2.38×10^{-10}	40
LDH(NO_3^-)/QPVA-20	21,830	1.32×10^{-9}	0.87	2.77×10^{-10}	50
LDH(NO_3^-)/QPVA-20	15,100	1.38×10^{-9}	0.87	2.76×10^{-10}	60
LDH(NO_3^-)/QPVA-20	12,470	1.71×10^{-9}	0.85	2.56×10^{-10}	70
LDH(NO_3^-)/QPVA-20	10,150	1.55×10^{-9}	0.86	2.56×10^{-10}	80
LDH(NO_3^-)	5,336	4.48×10^{-10}	0.96	2.61×10^{-10}	80
LDH(NO_3^-)/QPVA-10	8,237	2.19×10^{-9}	0.85	3.19×10^{-10}	80
LDH(NO_3^-)/QPVA-30	11,380	1.16×10^{-9}	0.89	2.89×10^{-10}	80
LDH(NO_3^-)/QPVA-40	16,390	9.18×10^{-10}	0.92	3.42×10^{-10}	80
LDH(Cl^-)/QPVA-20	20,260	9.94×10^{-10}	0.90	2.99×10^{-10}	80
LDH(OH^-)/QPVA-20	43,450	1.31×10^{-9}	0.76	5.98×10^{-11}	80
LDH(CO_3^{2-})/QPVA-20	56,570	9.91×10^{-11}	0.88	1.91×10^{-11}	80

a. $C = Y_o^{1/\alpha} R^{(1/\alpha-1)}$

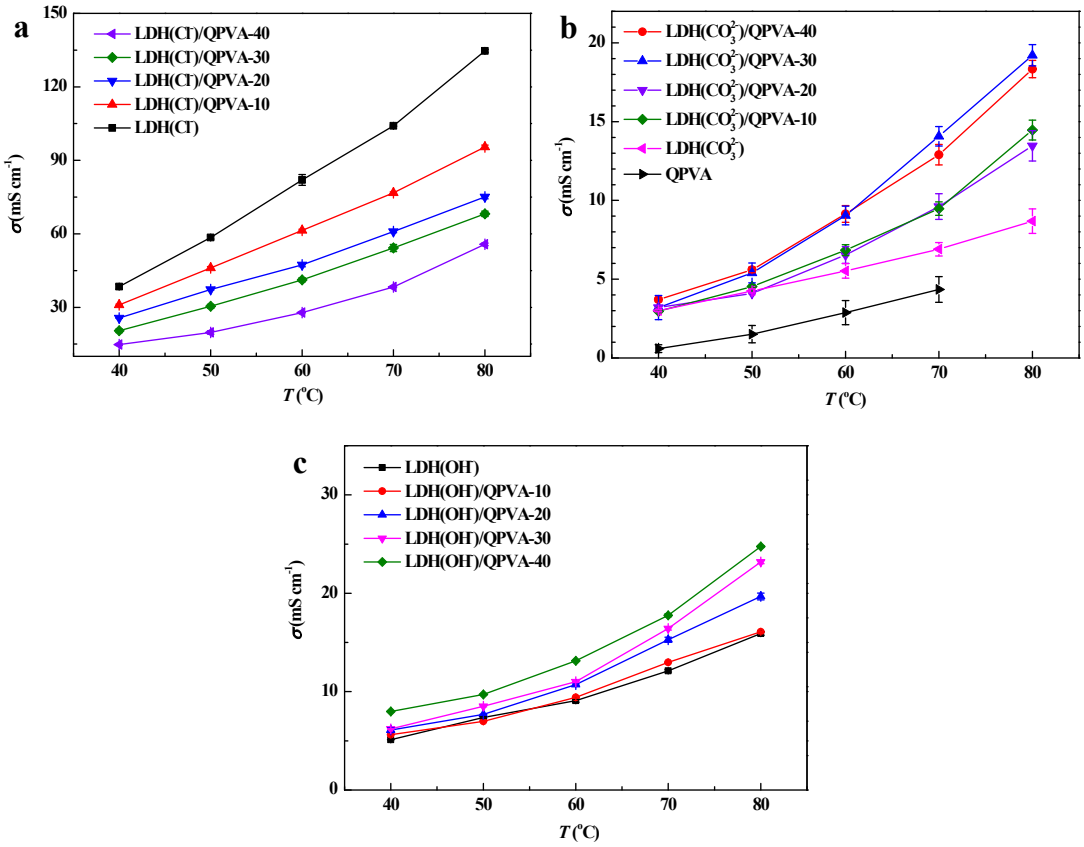

Fig. S16 (a) Temperature-dependent ion conductivity of LDH(Cl^-) and LDH(Cl^-)/QPVA membranes under 98% RH. (b) Temperature-dependent ion conductivity of QPVA, LDH(CO_3^{2-}) and LDH(CO_3^{2-})/QPVA membranes under 98% RH. The QPVA membrane was partially dissolved above 70 °C, which hindered its conductivity measurement at higher temperatures. (c) Temperature-dependent ion conductivity of LDH(OH^-) and LDH(OH^-)/QPVA membranes under 100% RH.

In Fig. S16a, the membranes intercalated with Cl^- also exhibited decreased anion conductivity with increasing amount of QPVA inside, whereas the membranes intercalated with CO_3^{2-} and OH^- exhibited different conductive performance with the incorporation of the polymer (Fig. S16b and 16c). Given the poor conductivity of the

membranes with CO_3^{2-} and OH^- intercalation, the anion conduction through the inter-laminate channels of LDH should not be neglected within the composite membranes. Fig. S16b illustrated enhanced anion conductivity of the LDH(CO_3^{2-})/QPVA membranes compared with the pure LDH(CO_3^{2-}) and the QPVA membranes, reflecting the contribution of the organic-inorganic interfaces to the conductive performance of the LDH(CO_3^{2-})/QPVA composites

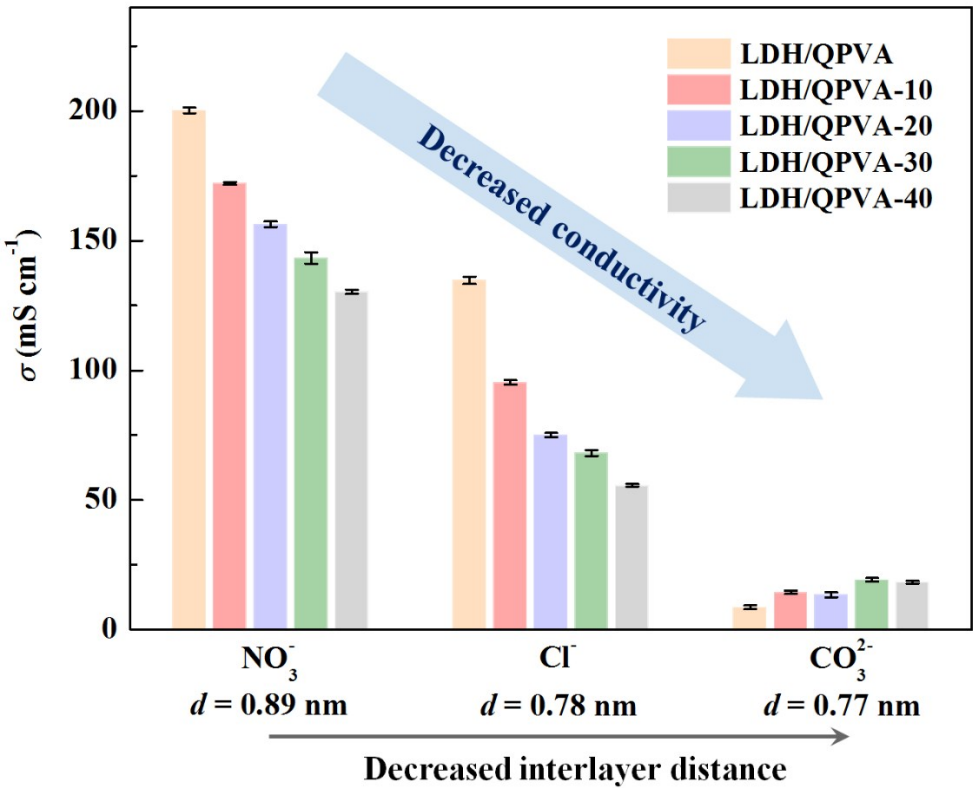

Fig. S17 Ion conductivity of the LDH-based membranes versus interlayer distance of restacked LDH nanosheets.

Table S3 Interaction energy between the host layer of LDH and interlayer anions

Samples	LDHs-CO_3^{2-}	LDHs-OH^-	LDHs-Cl^-	LDHs-NO_3^-
Interaction energy(eV)	-11.39[a]	-	-4.24[a]	-4.19[a]
	-	-6.34[b]	-5.44[b]	-
	-15.62[c]	-	-4.99[c]	-

[a.] Data in ref. S4; [b.] Data in ref S5; [c.] Data in ref S6

Table S4 Mechanical properties of the pure LDH membrane and composite membranes

Membrane	Tensile strength (MPa)	Young's modulus (GPa)	Elongation at break (%)	Toughness (MJ m^{-3})
LDH	16.5	1.28	2.3	0.22
LDH/QPVA-10	34.9	2.57	4.4	0.97
LDH/QPVA-20	48.4	2.60	6.6	2.09
LDH/QPVA-30	40.9	2.42	8.0	2.36
LDH/QPVA-40	34.0	1.68	8.9	2.11

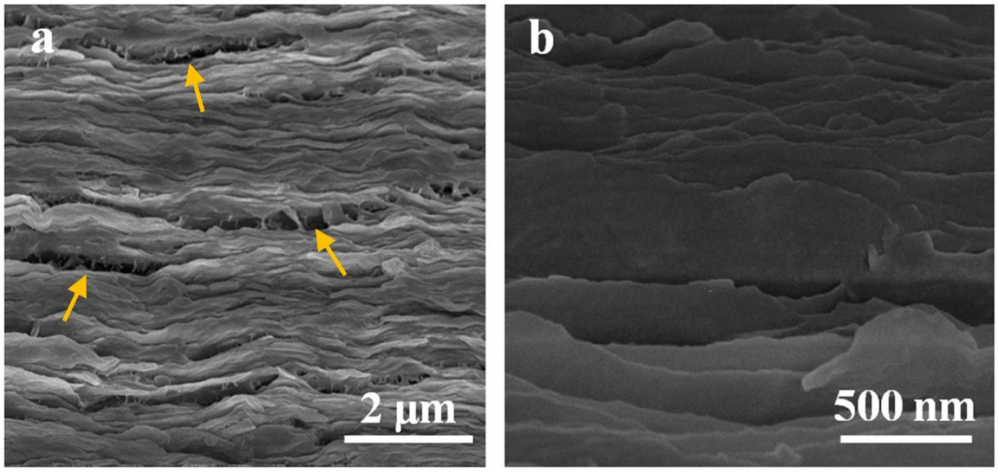

Fig. S18 (a) Cross-section and (b) front fracture morphology of the LDH/QPVA-20 membrane after tensile measurement. Voids (marked by arrows) could be observed from the cross-sections of the membrane. Both the cross-section and front fracture morphology showed that the LDH nanosheets were pulled out after stretching.

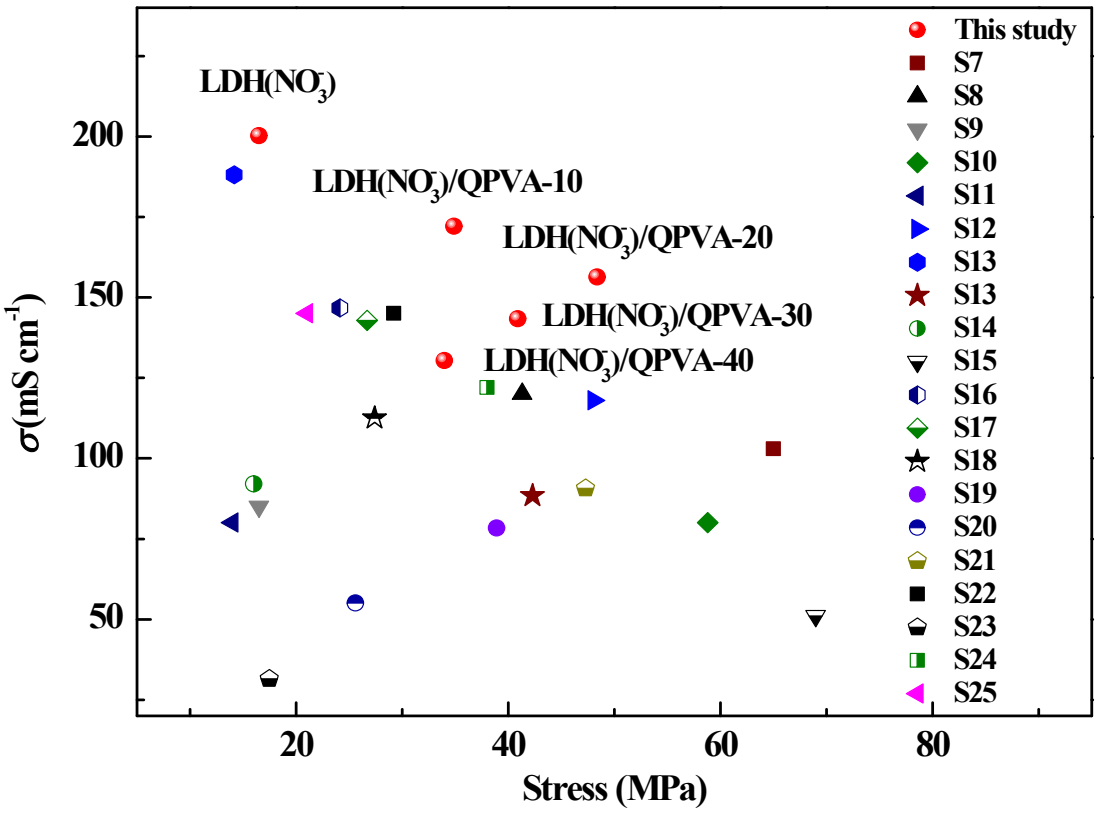

Fig. S19 Comparisons of mechanical strength and ion conductivity of the present membranes with anion exchange membranes reported in literatures.

Table S5 Comparisons of mechanical strength and ion conductivity of the present membranes with anion exchange membranes reported in literatures.

Membrane	σ [a] (mS cm^{-1})	Tensile strength (MPa)	Reference
XE-Imd60	103.3	65.0	S7
AI-PES-16	120.1	41.3	S8
DQAPS	84.7	16.5	S9
ImPPESN-0.8	79.8	58.8	S10
Membrane-5	80.2	14.0	S11
PEEK/QA-P(ES1-co-ES2)-5	118.6	47.9	S12
PSU/SiO_2-QPSt-70	188.1	14.2	S13
PSU/SiO_2-QPSt-20	88.4	42.3	S13
PAES-Q-90	92.1	16.0	S14
x-PP-DMHDA-20	51.1	69.0	S15
ImPESN-30-22	146.7	24.1	S16
TA-14C-1.21	142.8	26.7	S17
ImPES-0.45	112.5	27.4	S18
MM-PES-1.5-1	78.3	38.9	S19
TMImPPO	55	25.6	S20
ImPEEK/ImP-20	90.7	47.3	S21
LDPE-AEM(100 kGy)	145.0	29.2	S22
QPSF/5%LDH	31.5	17.5	S23
40-QA-LDH/TC-QAPPO	122.0	38	S24
pc-MBPPO	145.0	21	S25
LDH(NO_3^-)	200.2	16.5	
LDH(NO_3^-)/QPVA-10	172.1	34.9	
LDH(NO_3^-)/QPVA-20	156.3	48.4	This study
LDH(NO_3^-)/QPVA-30	143.3	40.9	
LDH(NO_3^-)/QPVA-40	130.3	34.0	

[a] The ion conductivity of the hydrated membranes were measured at 80 °C.

References

1. Y. Xiong, J. Fang, Q. H. Zeng and Q. L. Liu, *J. Membr. Sci.* , 2008, **311**, 319-325.

2. H.-S. Kim, Y. Yamazaki, J.-D. Kim, T. Kudo and I. Honma, *Solid State Ionics* 2010, **181**, 883-888.

3. N. Iyi, Y. Ebina and T. Sasaki, *Langmuir*, 2008, **24**, 5591-5598.

4. J. Liu and X. Zhang, *J. Fuel Chem. Technol.*, 2013, **41**, 761-768.

5. G. X. Pan, F. Cao, J. T. Yang, Z. M. Ni, P. S. Tang, H. F. Chen and S. S. Lv, *Adv. Mater. Res.*, 2011, **239-242**, 2293-2296.

6. G.-X. Pan, Z.-M. Ni and X.-N. Li, *Acta Phys. Chim. Sin.* , 2007, **23**, 1195-1200.

7. K. H. Lee, D. H. Cho, Y. M. Kim, S. J. Moon, J. G. Seong, D. W. Shin, J.-Y. Sohn, J. F. Kim and Y. M. Lee, *Energy Environ. Sci.* , 2017, **10**, 275-285.

8. A. H. N. Rao, S. Nam and T.-H. Kim, *J. Mater. Chem. A*, 2015, **3**, 8571-8580.

9. J. Pan, Y. Li, J. Han, G. Li, L. Tan, C. Chen, J. Lu and L. Zhuang, *Energy Environ. Sci.* , 2013, **6**, 2912-2915.

10. A. N. Lai, Y. Z. Zhuo, C. X. Lin, Q. G. Zhang, A. M. Zhu, M. L. Ye and Q. L. Liu, *J. Membr. Sci.* , 2016, **502**, 94-105.

11. T. Feng, B. Lin, S. Zhang, N. Yuan, F. Chu, M. A. Hickner, C. Wang, L. Zhu and J. Ding, *J. Membr. Sci.* , 2016, **508**, 7-14.

12. Z. Li, X. He, Z. Jiang, Y. Yin, B. Zhang, G. He, Z. Tong, H. Wu and K. Jiao, *Electrochim. Acta* 2017, **240**, 486-494.

13. G. He, M. Xu, Z. Li, S. Wang, S. Jiang, X. He, J. Zhao, Z. Li, X. Wu, T. Huang, C. Chang, X. Yang, H. Wu and Z. Jiang, *ACS Appl. Mat. Interfaces* 2017, **9**, 28346-28354.

14. X. Li, G. Nie, J. Tao, W. Wu, L. Wang and S. Liao, *ACS Appl. Mat. Interfaces* 2014, **6**, 7585-7595.

15. M. Zhang, J. Liu, Y. Wang, L. An, M. D. Guiver and N. Li, *J. Mater. Chem. A*, 2015, **3**, 12284-12296.

16. A. N. Lai, L. S. Wang, C. X. Lin, Y. Z. Zhuo, Q. G. Zhang, A. M. Zhu and Q. L. Liu, *ACS Appl. Mat. Interfaces* 2015, **7**, 8284-8292.

17. Q. Ge, J. Ran, J. Miao, Z. Yang and T. Xu, *ACS Appl. Mat. Interfaces* 2015, **7**, 28545-28553.

18. D. Guo, A. N. Lai, C. X. Lin, Q. G. Zhang, A. M. Zhu and Q. L. Liu, *ACS Appl. Mat. Interfaces* 2016, **8**, 25279-25288.

19. S. Kwon, A. H. N. Rao and T.-H. Kim, *J. Power Sources* 2018, **375**, 421-432.

20. Y. Zhu, Y. He, X. Ge, X. Liang, M. A. Shehzad, M. Hu, Y. Liu, L. Wu and T. Xu, *J. Mater. Chem. A*, 2018, **6**, 527-534.

21. Z. Li, Y. Zhang, T. Cao, Y. Yang, Y. Xiong, S. Xu and Z. Xu, *J. Membr. Sci.* , 2017, **541**, 474-482.

22. L. Wang, J. J. Brink, Y. Liu, A. M. Herring, J. Ponce-Gonzalez, D. K. Whelligan and J. R. Varcoe, *Energy Environ. Sci.* , 2017, **10**, 2154-2167.

23. W. Liu, N. Liang, P. Peng, R. Qu, D. Chen and H. Zhang, *J. Solid State Chem.* , 2017, **246**, 324-328.

24. N. Chen, C. Long, Y. Li, D. Wang and H. Zhu, *J. Membr. Sci.* , 2018, **552**, 51-60.

25. S. S. Nagarkar, B. Anothumakkool, A. V. Desai, M. M. Shirolkar, S. Kurungot and S. K. Ghosh, *Chem. Commun.* , 2016, **52**, 8459-8462.